Dynamic Theory of Liquid Junction Potentials

Edmund J. F. Dickinson, Leon Freitag, and Richard G. Compton*

Department of Chemistry, Physical and Theoretical Chemistry Laboratory, Oxford University, South Parks Road, Oxford, United Kingdom OX1 3QZ

Received: August 19, 2009; Revised Manuscript Received: November 18, 2009

A Nernst−Planck−Poisson finite difference simulation system is used to model the dynamic evolution of a liquid junction from a nonequilibrium initial condition to a condition of steady potential difference, in a linear semi-infinite space. Liquid junctions of Lingane's type 1 (monophasic, unequal concentration) and type 2 (bi-ionic potential; biphasic, equal concentration) are considered, for the sake of simplicity. Analysis of the results shows consistency with known and novel asymptotic solutions. A comprehensive dynamic theory of the free liquid junction potential is presented, having considered the simulated concentration profiles and electric field in the system. This reveals a dynamically relaxing junction in which a diffuse layer continues to expand. This is advocated as physically realistic and shown to be consistent with a steady state potential difference, which arises after 10−1000 ns for typical aqueous systems, when the expanding diffuse layer has a corresponding size of 10−1000 nm. Hence, Planck's concept [*Wied. Ann.* **1890**, *40*, 561−576] that a steady state potential difference exclusively implies a static junction with equal fluxes of all species is shown to be false, for an unconstrained system.

1. Introduction

1.1. The "Traditional" Liquid Junction. In the equilibration of spatially heterogeneous liquid systems where ionic species have unequal transport coefficients, a charge separation arises as a consequence of the diffusion of different species at differing rates. This charge separation causes an electric field in solution, and hence migration which accelerates the transport of the slower species and retards the transport of the more rapid species.

Such liquid junctions were formally classified into types 1−3 by Lingane:[1] Type 1 is a junction of two solutions of common phase but different concentration, type 2 is a junction of two solutions of different phase but common concentration, and type 3 is all other liquid junctions. To avoid undue complexity and to focus on the fundamental physical concepts involved, we shall study the dynamics of type 1 and 2 junctions only. These are exemplified respectively by the junction between two HCl(aq) solutions of different pH and by the junction between equimolar NaCl(aq) and KCl(aq) solutions. Figure 1 displays these liquid junctions.

In the traditional concept of a liquid junction, as developed more than 100 years ago by Nernst and Planck,[2−4] the electric field will develop in time until the fluxes of the two species are equal; the discrepancy in their diffusive flux arising from unequal transport coefficients is precisely balanced by their opposite migrational attraction. In this condition of equally rapid transport, no further charge separation occurs across the junction and so the potential difference across the space is constant.

This "steady state" condition is derived assuming, in general, arbitrary confinement of the junction to a boundary layer of finite length with Dirichlet boundaries (constant concentrations). Within this boundary layer, concentration profiles and potential vary linearly, such that the boundary layer is electroneutral and the Nernst−Planck equations may be taken at steady state. Such confinement may occur in a real system if there is an impermeable membrane or convectional Nernst layer, although in free solution such constraints ought not apply at a short time scale.[5]

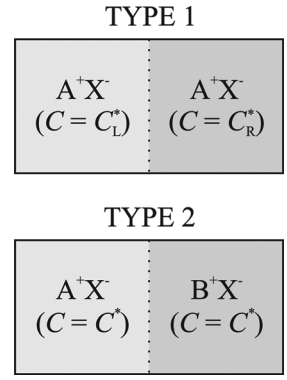

Figure 1. Lingane's type 1 and type 2 liquid junctions.

The Henderson equation,[6,7] which gives the magnitude of a liquid junction potential, E_{LJP}, as a function of the charges, z_i, diffusion coefficients, D_i, and concentrations, C_i, for all species i in the left (L) and right (R) phases of the junction, is derived thermodynamically assuming a linear boundary layer:[8]

$$E_{LJP} = \frac{\sum_i \frac{|z_i|D_i}{z_i}(C_{i,R} - C_{i,L})}{\sum_i |z_i|D_i(C_{i,R} - C_{i,L})} \frac{RT}{F} \ln \frac{\sum_i |z_i|D_i C_{i,L}}{\sum_i |z_i|D_i C_{i,R}} \quad (1.1)$$

where R is the gas constant, F is the Faraday constant, and T is the temperature; additionally, activity and concentration are taken to be interconvertible. The logic behind Planck's derivation of a transcendental equation for the liquid junction potential in the original literature,[4] and how this equation and Planck's assumptions relate to the Henderson equation, are summarized in Supporting Information A.

* Corresponding author. Fax: +44 (0) 1865 275410. Phone: +44 (0) 1865 275413. E-mail: richard.compton@chem.ox.ac.uk.

10.1021/jp908024s
Published on Web 12/10/2009

TABLE 1: Review of Work Concerned with Analysis and Simulation of Liquid Junction Potentials[a]

author	year	method	boundary	E/N	activity	comments
Nernst[2]	1889	An. NP	finite Dir.	yes	no	
Planck[3,4]	1890	An. NP	finite Dir.	yes	no	
Henderson[6,7]	1907−08	An. Thermo.	finite Dir.	yes	no	
Goldman[21]	1942	An. NP	finite Dir.	yes	no	finite membrane
Hafemann[10]	1965	Exp. NPP	Expg. Dir.	no	yes	
Hickman[15]	1970	An. NPP	Semi-inf. Dir.	no	no	$t \rightarrow \infty$
Goldberg et al.[22]	1972	Exp. NPP	finite Dir.	no	yes	Onsager equations
Jackson[16]	1974	An. NPP	Semi-inf. Dir.	no	no	$t \rightarrow \infty$
Morf[23]	1977	An. NP	finite Dir.	yes	no	mean mobilities
Brumleve et al.[24,25]	1978−81	Imp. NPP	finite Dir.	no	no	
Mafé et al.[26]	1986	Imp. NPP	finite Dir.	no	no	
Bagg[11−13]	1990−92	NI	Expg. Dir.	no	yes	
Horno et al.[27]	1992	network NP	finite Neu.	no	no	
Martuzans et al.[28]	1998	Imp. NPP	finite Neu.	no	no	
Skryl[18]	2000	Imp. NPP	finite Neu.	no	no	hyperbolic diffusion
Sokalski et al.[19,20]	2001−03	Imp. NPP	finite Dir.	no	no	membrane potentials
Josserand et al.[29]	2003	2D FEM NP	finite Neu.	yes	no	microchannel flow
Park et al.[30]	2006	LB NPP	finite Neu.	no	no	microchannel flow
Perram et al.[14]	2006	Imp. NPP	finite Neu.	no	no	
Filipek et al.[31]	2009	Imp. NPP	finite Neu.	no	no	membrane potentials
this work	2009	Imp. NPP	Semi-inf. Dir.	no	no	

[a] Abbreviations: E/N, electroneutrality approximation; An., analytical; Exp., explicit finite difference; Imp., implicit finite difference; NI, numerical integration; FEM, finite element method; LB, lattice Boltzmann method; NP, Nernst−Planck; NPP, Nernst−Planck−Poisson; Thermo., thermodynamic; Dir., Dirichlet; Neu., Neumann; Expg., expanding; Semi-inf., semi-infinite.

In the type 1 case, for a monovalent electrolyte A^+X^-, the Henderson equation reduces to

$$(t_A - t_X)\frac{RT}{F}\ln\frac{C_L^*}{C_R^*} \tag{1.2}$$

where

$$t_i = \frac{D_i}{D_A + D_X} \tag{1.3}$$

and i is A or X.

In the type 2 case, for monovalent electrolytes A^+X^- and B^+X^-, the Henderson equation reduces to

$$E_{LJP} = \frac{RT}{F}\ln\frac{D_A + D_X}{D_B + D_X} \tag{1.4}$$

1.2. Past Computational Studies. Guggenheim[9] (1930) defined the Planck model as a "constrained" liquid junction, as diffusion is limited by the finite boundaries; the "free" liquid junction, in which the diffuse layer may expand to infinity, was recognized as more physically realizable for a simple liquid−liquid contact in a cell but was sadly theoretically intractable before the advent of digital computation. Consideration of Planck's original work[4] would suggest that the finite boundary layer was invoked for reasons of mathematical necessity rather than physical insight. In particular, Guggenheim wrote that "The physical conditions corresponding to the Planck formula have not generally been understood", and except for identification of cases where some tangible boundary does limit diffusion, there is scant evidence in the literature that this situation has improved since 1930; since the 1960s, the simulation of liquid junction potential formation has been studied extensively but almost always with the imposition of finitely positioned boundary conditions. Numerical simulation work to date is summarized in Table 1: probably those studies most similar to this work are those by Hafemann[10] and Bagg,[11−13] in which the computed grid of points was allowed to grow to avoid constrained diffusion but in neither case were the results analyzed in their physical context.

In the recent extensive study of Perram et al.,[14] the assumptions made in the traditional derivation of the Henderson equation, and in most past simulations, were eloquently denounced as unphysical: electroneutrality at finite time is dynamically inconsistent with solutions where the Poisson equation is obeyed, and the replenishment of material to constant concentration at a finitely positioned boundary is not consistent with the laws of conservation of mass, unless a convectional Nernst layer is arbitrarily invoked. Their proposed alternative employed Neumann boundary conditions at finite boundaries, thus maintaining conservation of mass but still confining the study to a "constrained" junction. The authors found that a pseudo-steady-state potential difference is maintained so long as bulk solution remains available, and that the characteristic and constant potential arising from the charge separation achieved at this pseudo-steady state is equivalent to that predicted by classical theory. Since the junction was constrained, all liquid junction potentials observed were necessarily transient and collapsed as the diffuse layer around the junction encountered the Neumann boundaries.

1.3. Scope and Context of This Work. In an electrochemical cell, among other contexts, the bulk solution on either side of a liquid junction is typically extensive, yet the dynamics of "free" liquid junction formation, independent of the cell size and neglecting convection, are not yet well established. In this paper, we shall analyze and rationalize trends in the dynamics of liquid junctions, as a function of diffusion coefficients, bulk concentrations, and other pertinent system variables.

We shall consider a junction where two solutions of different concentration or phase begin in direct contact, with step functions describing the concentration of each species. The Nernst−Planck−Poisson equations are solved numerically, ensuring a complete dynamic electrostatic treatment that maintains conservation of charge. The outer (bulk) boundary conditions are of the Dirichlet type but are semi-infinite in extent, such that the distance considered on either side of the junction always exceeds the maximum possible extent of the diffusion layer. Hence, conservation of mass is maintained everywhere,

and material is not replenished close to the junction in an unphysical manner, as with a finite Dirichlet boundary. Additionally, the availability of bulk solution is implicitly infinite, so diffusion is not constrained: the pseudo-steady state will not collapse as a result of a finite simulation space and so the results will yield suitably general trends.

Our simulations agree well at long times with the insightful time-to-infinity asymptotic analysis of the free junction by Hickman and Jackson,[15,16] and hence confirm the physical picture implied by the (mathematical) conclusions of these authors. We additionally develop a short time asymptotic treatment, which also agrees well with simulation; the dynamic transition between these asymptotic behaviors is also revealed by numerical simulation, and the characteristic time and space scales at which the long time asymptotic behavior is attained are recovered as system variables.

The principal aim of this work will be to demonstrate the novel physical insight that the liquid junction potential is best understood as resulting from a dynamically *moving* junction of varying charge and size. It will be demonstrated that Planck's assumption of a static boundary layer, made in order to invoke a steady-state expression for concentration, is superfluous: a time-independent liquid junction potential will arise even for a continuously diffusing, non-steady-state system. Despite the success of the Henderson equation, the static Nernst−Planck−Henderson model is unphysical in several respects—local electroneutrality, confinement of the diffuse layer, and unphysical replenishment of material at a finite boundary—and where diffusion is not tangibly constrained, such a model cannot be representative of the reality of the free liquid junction.

2. Theoretical Model

2.1. Establishment of the Model. We consider a planar junction, perpendicular to a linear coordinate x, between two solutions of binary monovalent electrolyte. The solutions are homogeneous in all planes parallel to the junction, and so mass transport in all axes but x is neglected. At the point $t = 0$, some imagined barrier at the junction is removed, allowing the solutions to diffuse freely into each other.

The flux of any species i for i = A, B, or X at any point in solution may be described by the Nernst−Planck equation. Assuming no bulk flow or convection, the equation can be expressed as a sum of two terms, the first being a diffusional contribution and the second a migrational contribution:

$$J_i = -D_i\left(\frac{\partial C_i}{\partial x} + \frac{z_i F}{RT} C_i \frac{\partial \phi}{\partial x}\right) \tag{2.1}$$

where J_i is the x-component of the flux vector for species i, ϕ is the potential, and all other terms are defined as above. In all of the discussion below, we assume the continuum Nernst−Planck equation to be accurate, the fluxes of different ions to be independent of each other, and D_i to not be a function of concentration; i.e., microscopic single ion effects are neglected.[17]

By conservation of mass, the space-time evolution of C_i is given by

$$\frac{\partial C_i}{\partial t} = -\frac{\partial J_i}{\partial x} \tag{2.2}$$

and so

$$\frac{\partial C_i}{\partial t} = D_i\left(\frac{\partial^2 C_i}{\partial x^2} + \frac{z_i F}{RT}\frac{\partial}{\partial x}\left(C_i \frac{\partial \phi}{\partial x}\right)\right) \tag{2.3}$$

The potential at any point in solution must further satisfy the Poisson equation:

$$\frac{\partial^2 \phi}{\partial x^2} = -\frac{\rho}{\varepsilon_s \varepsilon_0} \tag{2.4}$$

where ε_s is the dielectric constant of the solvent medium, ε_0 is the permittivity of free space, and ρ is the local charge density, achieved by summing the charges of all species present multiplied by their respective concentrations:

$$\rho = F\sum_i z_i C_i \tag{2.5}$$

Rewriting in a homogeneous form, we obtain a system of equations, called the Nernst−Planck−Poisson (NPP) equation set:

$$\left(\frac{\partial^2 C_i}{\partial x^2} + \frac{z_i F}{RT}\frac{\partial}{\partial x}\left(C_i \frac{\partial \phi}{\partial x}\right)\right) - \frac{1}{D_i}\frac{\partial C_i}{\partial t} = 0 \tag{2.6}$$

for each species i, and

$$\frac{\partial^2 \phi}{\partial x^2} + \frac{F}{\varepsilon_s \varepsilon_0}\sum_i z_i C_i = 0 \tag{2.7}$$

The NPP system will be used in this form throughout the following study.

2.2. Normalization. To reduce the number of independent variables in the system and to simplify the NPP equations, dimensionless coordinates are introduced. Concentration is normalized against the bulk concentration of a chosen normal species on the right side of the junction (conventionally X for types 1 and 2), and the potential is expressed in units of RT/F:

$$c_i = \frac{C_i}{C^*_{\mathrm{X,R}}} \tag{2.8}$$

$$\theta = \frac{F}{RT}\phi \tag{2.9}$$

The diffusion coefficients are normalized against the diffusion coefficient of species X:

$$D'_i = \frac{D_i}{D_{\mathrm{X}}} \tag{2.10}$$

and dimensionless time and space coordinates are defined as

$$X = k \cdot x \tag{2.11}$$

$$\tau = k^2 \cdot D_{\mathrm{X}} \cdot t \tag{2.12}$$

where

$$k^2 = \frac{F^2 C^*_{\mathrm{X}}}{RT\varepsilon_s \varepsilon_0} \tag{2.13}$$

We then obtain the NPP equation set in dimensionless coordinates:

$$\frac{\partial^2 c_i}{\partial X^2} + z_i \frac{\partial}{\partial X}\left(c_i \frac{\partial \theta}{\partial X}\right) - \frac{1}{D'_i}\frac{\partial c_i}{\partial \tau} = 0 \tag{2.14}$$

$$\frac{\partial^2 \theta}{\partial X^2} + \sum_i z_i c_i = 0 \tag{2.15}$$

The physical meaning of k may be identified by considering the conventional definition of the Debye length x_{D}, giving the mean radius of an ionic atmosphere, for a binary electrolyte as

$$x_D = \sqrt{\frac{RT\varepsilon_s\varepsilon_0}{2F^2C^*}} = \frac{k^{-1}}{\sqrt{2}} \tag{2.16}$$

The time-dependent solutions of the NPP equations are functions of X and τ only, for any given boundary conditions, and the dimensional solutions then scale by k and D_X.

2.3. Boundary Conditions. The NPP equations must be solved subject to suitable boundary conditions. The outer boundaries are defined to be semi-infinite, such that they will vastly exceed the diffusion layer throughout the simulation time. The maximum value of X used in the simulation, X_{max}, is therefore defined as $6(D_i' \cdot \tau_{max})^{1/2}$, where i is the species with the greatest diffusion coefficient and τ_{max} is the maximum τ value for the simulation, given as a parameter. This allows us to treat the problem of a free liquid junction using only a finite simulation space, as whatever τ_{max} is chosen, the simulation space is sufficiently large to ensure that no flux or field will arise outside the boundaries of the space and so the boundary position does not constrain the evolution of the system.

We assume that the concentrations of the ions at the boundaries are constant, and equal to their bulk values (Dirichlet boundary conditions), i.e., for all τ:

$$X \to +\infty \qquad c_i = c_{i,R}^* \tag{2.17}$$

$$X \to -\infty \qquad c_i = c_{i,L}^* \tag{2.18}$$

As for $\tau > 0$, there is no exchange of material at the boundaries, and the system is electroneutral at $\tau = 0$, the simulation space is a Gaussian box of zero enclosed charge. Therefore, the electric field is zero at the boundaries, again at all τ:

$$X \to \pm\infty \qquad \frac{\partial\theta}{\partial X} = 0 \tag{2.19}$$

2.4. Numerical Methods. Details of the numerical methods employed are supplied in Supporting Information B. In brief, a fully implicit method is used for simulation, over a grid of points expanding in both space directions from the initial junction position, $X = 0$. The resulting set of nonlinear simultaneous equations is solved at each time step using the iterative Newton−Raphson method, with the time step length also expanding with increasing τ. Appropriate parameters were established with a convergence study.

All simulations were programmed in C++, compiled with GNU gcc with optimization level 3, and run on a desktop computer with an Intel Core2 Quad 2.4 GHz processor and 3.2 GB of RAM, with typical runtimes of 3−5 h per simulation due to the high convergence demands of the system.

3. Theoretical Results and Discussion

3.1. Simulated Limiting Potentials. Simulated liquid junction potentials were achieved by continuing a dynamic simulation until some τ where the potential is approximately constant. These simulated potentials were compared with the established Henderson equation, in order to demonstrate the general convergence of the simulation.

3.1.1. Type 1 Liquid Junction Potentials. Type 1 liquid junctions were simulated for the cases $D_A' = 0.4$, 0.6, 0.8, and 0.9, as well as the special case of HCl, where $D_A' \approx 4.582$ (at infinite dilution, 298 K) in water.[8] Concentration ratios of $c_L^* = 10^{-0.1}$, $10^{-0.5}$, 10^{-1}, $10^{-1.5}$, and 10^{-2} were considered. Limiting junction potentials were recorded at a time where

$$0.998 \cdot |\Delta\theta_{LJP}(\tau)| \le |\Delta\theta_{LJP}(\tau/2)| \tag{3.1}$$

i.e., the potential difference between the two phases has reached an approximately constant value. Strong agreement (<0.25%) with the Henderson equation was observed in all cases (plots in Supporting Information C).

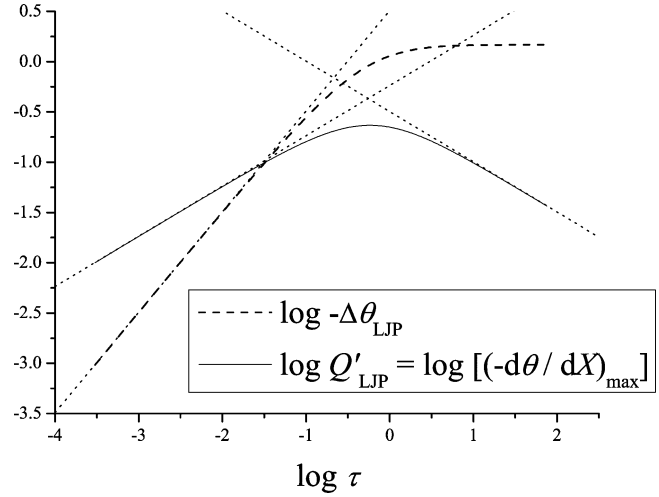

Figure 2. Dynamic evolution of liquid junction potential ($\Delta\theta_{LJP}$) and maximum electric field ($(-\partial\theta/\partial X)_{max}$) for the type 1 junction of 1 and 10 mM HCl(aq), plotted on a logarithmic scale in time. Asymptotic limits derived using a zero-feedback approach ($\tau \to 0$) and Boltzmann transform asymptotic analysis ($\tau \to \infty$) are plotted against the simulation data.

3.1.2. Type 2 Liquid Junction Potentials. Type 2 liquid junctions were simulated for the cases D_A' and $D_B' = 0.5$, 0.75, 1, 1.5, and 2, as well as the special cases of HCl/KCl and NaCl/KCl, with the condition for steady state as above (eq 3.1). Agreement (<0.8%) with the Henderson equation was observed in all cases (plots in Supporting Information C); we note here that the work of Hickman[15] showed that the Henderson equation is *not* exact for type 2 and so it is possible that the simulation shows higher accuracy compared to the "true" value for the liquid junction potential.

3.2. Dynamics of Liquid Junction Potential Formation: An Exemplar Type 1 Junction with HCl(aq). The dynamics of liquid junction formation were investigated for a concentration discontinuity in an aqueous solution of HCl from 1 mM (pH ≈ 3) to 10 mM (pH ≈ 2).

3.2.1. Trends in $\Delta\theta_{LJP}$ and ξ_{max}. The potential difference for the HCl system, $\Delta\theta_{LJP}$, is plotted as a function of τ on a logarithmic scale to demonstrate its development (Figure 2). The maximum electric field, $-\xi_{max} = (-\partial\theta/\partial X)_{max}$, is also plotted. The maximum electric field is plotted in place of the field at $X = 0$, as these are not equivalent. As will be detailed below, the maximum electric field gives the degree of charge separation in the junction, according to Gauss's law, and therefore is crucial in analyzing the potential difference across the junction; the position where this maximum field occurs is not fixed to $X = 0$ but rather is found to diffuse together with the species themselves.

These plots demonstrate that the electric field associated with unequal mass transport of H^+ and Cl^- ions achieves a maximum at $\tau \approx 0.5$; in dimensional units, the maximum field is ≈1.3 MV m^{-1} at ≈5 ns after contact between the solutions. Prior to this time, as time tends to zero, the potential difference is increasing proportionally to τ, and the maximum field increases proportionally to $\tau^{1/2}$. After the electric field reaches its critical limiting value, which scales with k and hence is a function of the ionic strength and permittivity of the solution, the electric field does *not* become constant but rather relaxes as $\tau^{-1/2}$, and the potential difference approaches the Henderson limiting value at long time, although the electric field continues to decay.

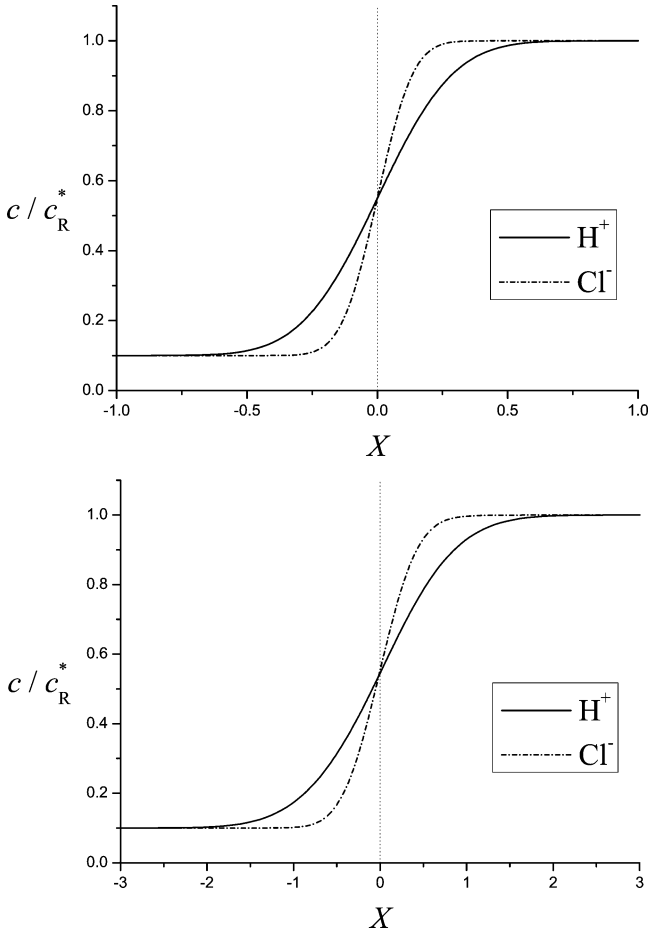

Figure 3. Concentration profiles for the HCl(aq) system at times $\tau = 0.01\tau_{trs}$ and $\tau = 0.1\tau_{trs}$ following junction formation. In the former, the junction is predominantly symmetric and resembles the independent diffusion-only case; in the latter, the point of isoconcentration has begun to move away from $X = 0$, although symmetry still dominates.

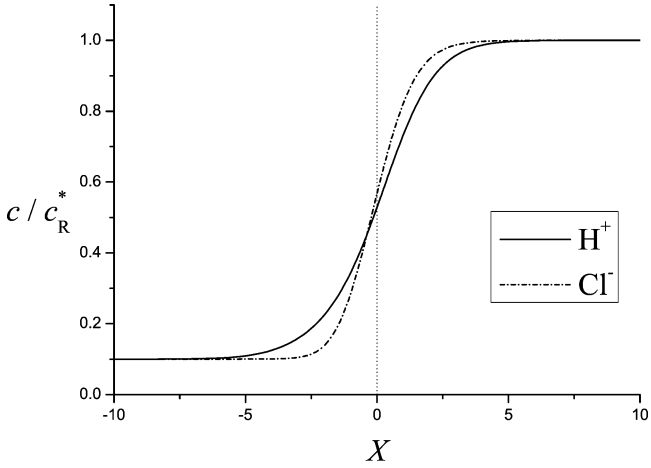

Figure 4. Concentration profiles for the HCl(aq) system at a time $\tau = \tau_{trs}$ following junction formation. Here, the field is maximal; the profiles show substantial asymmetry, and the point of isoconcentration has moved perceptibly away from $X = 0$.

Defining τ_{trs} as the characteristic transition time where the maximum field at the junction occurs, concentration profiles were recorded at a logarithmic range of times from $\tau = 10^{-2}\tau_{trs}$ to $\tau = 10^{2}\tau_{trs}$. These are shown at Figures 3−5. The evolution of the associated dimensionless electric field, $-\xi$, is also shown at Figure 6. It is evident that, at longer times, the position of maximum field in the system is mobile and moves away from

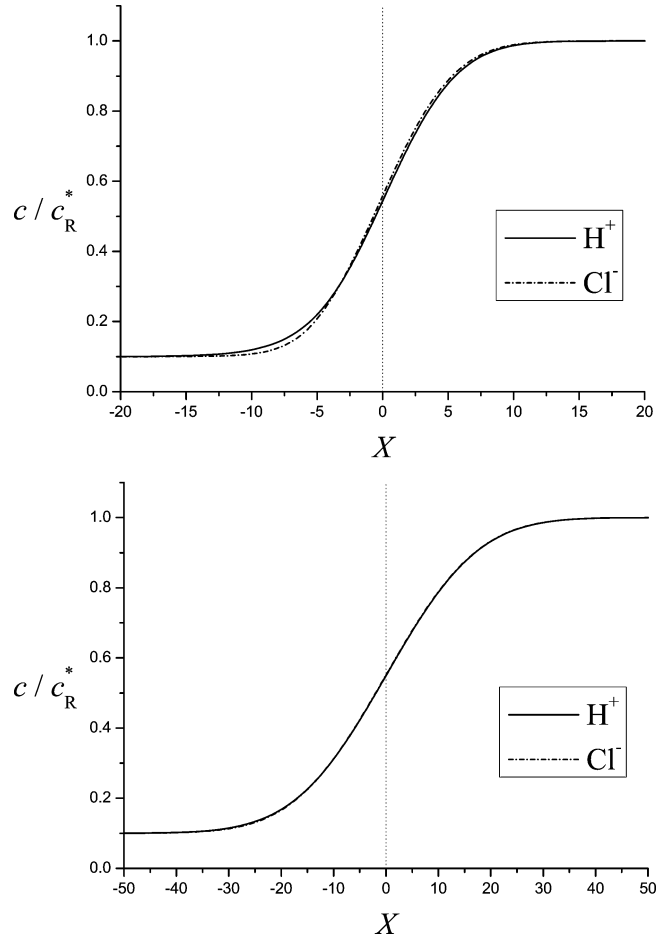

Figure 5. Concentration profile for the HCl(aq) system at times $\tau = 10\tau_{trs}$ and $\tau = 100\tau_{trs}$ following junction formation. In the former, electroneutrality is increasing in the system and symmetry is returning, although the point of isoconcentration continues to recede from $X = 0$. In the latter, the overall profile appears electroneutral, but in fact, a finite charge separation still exists which is maintaining a steady potential difference as the junction grows; close examination shows the point of isoconcentration to be continuously diffusing.

the initial position of the junction; additionally, the concentration profiles become increasingly asymmetric in this range. The significance of the position of maximum field in the system may be recognized as follows.

3.2.2. The Liquid Junction as a Gaussian Box Electrolytic Capacitor. The point of maximum electric field, $X_{MaxField}$, occurs where $\partial^2\theta/\partial X^2 = 0$, and hence, from eq 2.15, where $c_A = c_X$, excluding the trivial cases $X = \pm\infty$. Here, we recall Gauss's law, which states that the electric field at the surface of a charged volume is proportional to the charge within it:

$$\frac{\partial\theta}{\partial X} = -\bar{Q}_{enc} \tag{3.2}$$

where

$$\bar{Q}_{enc} = \frac{\bar{q}_{enc}}{C_X^* \varepsilon_s \varepsilon_0 RT} \tag{3.3}$$

and where $\bar{q}_{enc}$ is the enclosed charge per unit area (C m^{-2}).

Considering the Gaussian boxes contained within $-\infty < X < X_{MaxField}$ and $X_{MaxField} < X < +\infty$, we note that the electric field is zero, for reasons of symmetry or conservation of charge, at all boundaries of the boxes other than their junction. Therefore, as shown in Figure 7, $X_{MaxField}$ represents the position of overall charge separation, as the solution charge on one side of this

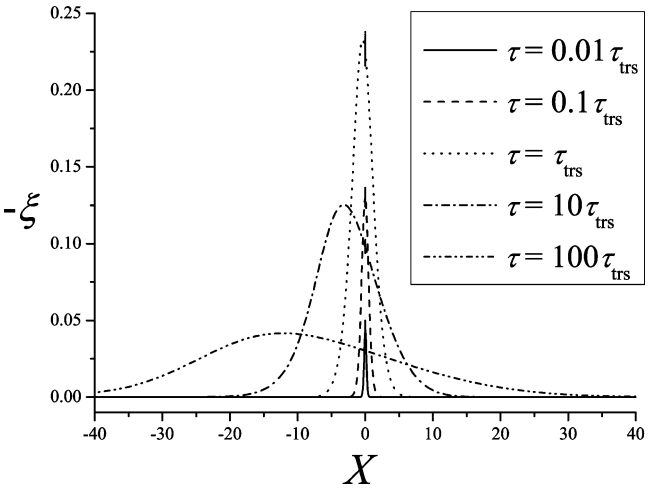

Figure 6. Evolution of the electric field profile for the HCl(aq) system at times $\tau = 0.01\tau_{trs}$ to $\tau = 100\tau_{trs}$ following junction formation. Increased asymmetry and the movement of X_{LJP}, the position of maximum field, away from the initial junction position are both evident. Some spikes result from errors in numerical differentiation owing to the high mesh density employed.

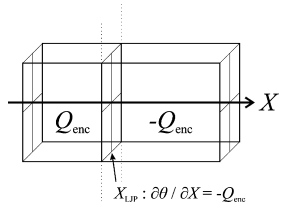

Figure 7. Representation of the liquid junction as two adjoining Gaussian boxes with equal and opposite charge.

point is equal and opposite to the solution charge on the other side. $X_{MaxField}$ may therefore be termed the *liquid junction position* and denoted X_{LJP}.

The liquid junction may now be discussed as a type of parallel plate capacitor, where the plates represent the volumes of solution on either side of X_{LJP}, which have dimensionless charges of $\pm(\partial\theta(X = X_{LJP})/\partial X)$. This "capacitor" charges and discharges spontaneously in time, with an associated potential difference from which the "capacitance" of the system may be inferred. From Figure 2, it is clear that the "capacitor" discharges to zero (at infinite time) without any alteration of its potential difference. At $\tau < \tau_{trs}$, the flux of H^+ across the junction is greater than the flux of Cl^- (charging), but at $\tau > \tau_{trs}$, these fluxes are *not* equal, but rather the flux of Cl^- is now greater than that of H^+ (discharging).

The simulated motion of this junction position, X_{LJP}, is plotted logarithmically against time at Figure 8, which shows that, in the short time limit, it moves from its initial position as $\tau^{3/2}$, and at long time as $\tau^{1/2}$.

3.2.3. Asymptotic Analysis at $\tau \rightarrow 0$ by a Zero-Feedback Approximation. The $\tau \rightarrow 0$ limiting behaviors of the type 1 liquid junction may be better understood by means of asymptotic analysis. To consider the low τ limit, we approximate that the migrational flux is zero and analyze the electric field arising from diffusion-only mass transport, ignoring the feedback of that field. The solutions to the diffusion equation, ignoring migration, are substituted into the Poisson equation, which is integrated to find an approximate electric field (mathematical details at Supporting Information D). The major predicted results are

$$\left.\frac{\partial\theta}{\partial X}\right|_{max} \approx \frac{1 - c_L^*}{\sqrt{\pi}}(1 - \sqrt{D'_A})\cdot\sqrt{\tau} \qquad (3.4)$$

$$\Delta\theta_{LJP} \approx (1 - c_L^*)(1 - D'_A)\cdot\tau \qquad (3.5)$$

which are plotted as the $\tau \rightarrow 0$ asymptotes in Figure 2, with evident agreement in both cases with simulation in this limit.

3.2.4. Asymptotic Analysis as $\tau \rightarrow \infty$ by Solution as a Power Series. Hickman[15] introduced $\tau \rightarrow \infty$ asymptotic analysis as a means of deriving the Henderson equation without recourse to electroneutrality; the $\xi_{max} \propto \tau^{-1/2}$ relaxation of the junction was correctly identified in following work by Jackson[16] and the observation of a constant potential rationalized, as here, in terms of the expansion of the junction. Their work is summarized for the type 1 case in Supporting Information F and G, and then extended to a novel analysis of the long time behavior of X_{LJP} and $\bar{Q}_{enc}$.

The following expressions for electric field and liquid junction potential arise from the theory as the leading nonzero term of the approximation as $\tau \rightarrow \infty$:

$$\xi = \frac{\partial\theta}{\partial X} \approx \frac{\beta\delta_2}{\sqrt{\delta_1\pi\tau}}\cdot\frac{e^{-z^2\delta_1/4}}{\gamma + \mathrm{erf}\left(\frac{z\sqrt{\delta_1}}{2}\right)} \qquad (3.6)$$

where $z = X/\sqrt{\tau}$, β is as above, and

$$\delta_1 = \frac{\frac{1}{D'_A} + 1}{2}; \qquad \delta_2 = \frac{\frac{1}{D'_A} - 1}{2}; \qquad \gamma = \frac{1 + c_L^*}{1 - c_L^*} \qquad (3.7)$$

and

$$\Delta\theta_{LJP} = \frac{\delta_2}{\delta_1}\ln\left|\frac{\gamma + 1}{\gamma - 1}\right| \qquad (3.8)$$

The latter expression is simply the Henderson equation for type 1. The validity of the former expression may be confirmed by comparison with a simulated electric field profile taken at long time; a very close agreement is observed, with the plot available in Supporting Information G.

Further, we note that, by Gauss's law, the position X_{LJP} occurs where

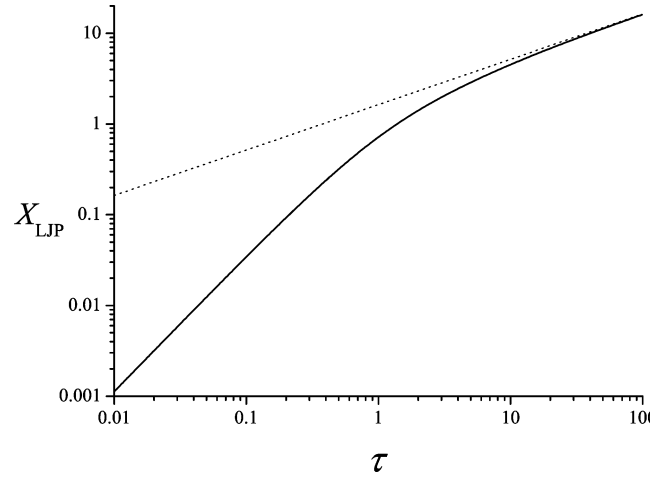

Figure 8. Evolution of the position of the liquid junction, X_{LJP}, for the HCl system, together with the long time behavior predicted by asymptotic analysis.

$$\frac{\partial^2\theta}{\partial X^2} = 0 \tag{3.9}$$

On differentiation of the time-dependent eq 3.6 (Supporting Information G), we find that X_{LJP} occurs where

$$\gamma + \mathrm{erf}(s) + \frac{e^{-s^2}}{s\cdot\sqrt{\pi}} = 0 \tag{3.10}$$

where

$$s = X\cdot\sqrt{\frac{\delta_1}{4\tau}} \tag{3.11}$$

Equation 3.10 is not, to our knowledge, invertable. It is single-valued and finite, however, for all $\gamma > 1$, and so its roots, $s(\gamma)$, may be evaluated numerically in this range. It follows that

$$X_{LJP} = s(\gamma)\cdot\sqrt{\frac{4\tau}{\delta_1}} \propto \tau^{1/2} \tag{3.12}$$

Asymptotic agreement with simulation for the junction position is again achieved, as shown at Figure 8.

The substitution of the identity eq 3.10 back into eq 3.6 yields the result

$$-\xi(X_{LJP}) = \bar{Q}_{enc} \approx \frac{\delta_2\cdot s(\gamma)}{\sqrt{\delta_1\tau}} \tag{3.13}$$

which demonstrates that the liquid junction is in a state of continuous loss of charge at a rate $\rightarrow \tau^{-1/2}$ as $\tau \rightarrow \infty$. This expression is plotted as an asymptote in terms of maximum electric field at Figure 2, showing very strong agreement with simulation.

3.2.5. The Liquid Junction Spatial Extent ΔX_θ. We define the junction spatial extent, ΔX_θ, as

$$\Delta X_\theta = X\left((\theta(\infty) - \theta(X)) = \frac{\Delta\theta_{LJP}}{100}\right) - X\left((\theta(X) - \theta(-\infty)) = \frac{\Delta\theta_{LJP}}{100}\right) \tag{3.14}$$

This is an effective measure of the range of nonzero electric field, and hence of the range over which charge separation in the liquid junction occurs. ΔX_θ is plotted on a logarithmic scale against τ at Figure 9. We observe that the junction initially grows as $\tau^{1/2}$; its growth then slows around the time when the field is maximum, before accelerating again toward a $\tau^{1/2}$ dependency at long times.

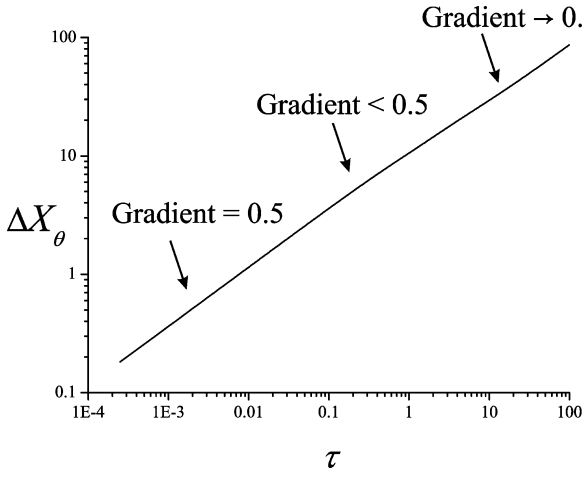

Figure 9. The junction spatial extent ΔX_θ as a function of τ on a logarithmic scale, for the HCl system, showing regions of "diffusive" expansion as $\tau^{1/2}$.

3.2.6. Conclusion on Type 1 Dynamics. A dynamical theory must therefore account for the short time trends, and for the following observations, which are inconsistent with the static concept of the liquid junction at long time: (a) the potential approaches a limiting value but the electric field does not; (b) the concentration profiles become asymmetric; (c) the liquid junction position, being the point of electroneutrality, moves away from its initial position; (d) the range of nonzero electric field continues to grow in τ. The agreement of simulation with asymptotic theory in both limits, as well as the provision, by simulation, of data concerning the dynamic transition between these two conditions, affords us a comprehensive understanding of the type 1 liquid junction potential.

At very small times, the electric field in solution does not yet strongly influence the mass transport of the A and X species; their migrational flux is negligible and so their concentration profiles approximately obey the diffusion equation. The field arising from unequal diffusion develops proportionally to diffusion through the junction, i.e., as $\tau^{1/2}$; equivalently, the total charge separation in the junction is increasing as $\tau^{1/2}$. The diffuse layer on either side of $X = 0$ is also developing as $\tau^{1/2}$, as shown by the trends in ΔX_θ. Under these conditions, we may imagine the junction as a parallel-plate capacitor where the separation, d, of the plates, being the separation of the positions of mean charge on either side of the junction, is growing as $\tau^{1/2}$. In a simplistic sense, we may assume a constant solution "capacitance", $\bar{C}_d$, which is a function of k, D'_A, and c^*_L, and hence

$$\frac{\partial\bar{Q}_{enc}}{\partial\Delta\theta_{LJP}} \propto \frac{\bar{C}_d}{d} \quad \therefore \quad \Delta\theta_{LJP} \propto (\bar{Q}_{enc}\cdot d) \propto (\tau^{1/2}\cdot\tau^{1/2}) \propto \tau \tag{3.15}$$

as is predicted by the asymptotic $\tau \rightarrow 0$ study. That is, at small times, diffusion causes a linear growth in junction potential as an increasing charge of magnitude $\propto \tau^{1/2}$ is being separated by an increasing distance $\propto \tau^{1/2}$.

The growing electric field must, however, impact upon the mass transport of A and X. The predicted movement of $X_{LJP} \propto \tau^{3/2}$ is evidence that there are tangible migration effects on the junction at all times $\tau > 0$. As the electric field increases, transport of the leading species (that with higher diffusion coefficient) is retarded and that of the following species (that with lower diffusion coefficient) is accelerated. The electric field is not uniform through the junction, however, but is maximal at the junction center and falls away to zero at either side. Therefore, the discrepancy in migrational flux between A and X, and hence the compensation for their differing rates of diffusion, is greater at the junction center than either in the region of lower concentration to the left *or* the region of higher concentration to the right. This causes a "bunching" of the junction: the leading species profile is squashed to the right and stretched to the left, and vice versa for the following species, such that the junction position itself moves with diffusion away from its initial position and hence the field becomes asymmetric. This is best observed in the concentration profiles recorded at maximum field (Figure 4).

The junction continues to charge as long as the flux of the leading species is greater than that of the following species, but this charging increases the electric field and so the rate of charging must gradually slow. The rate of charging falls to zero, i.e., equal fluxes of both species at the junction, at a characteristic time τ_{trs}, which is a function of D'_A and c^*_L. For typical

values of these parameters and a typical value of k, t_{trs} is of the order of 5−50 ns. Under a condition of equal fluxes, Planck argued that the potential difference across the junction is constant,[4] but as the junction charge is constant, this can then only be true if the mean distance of charge separation in the junction is also constant; where the diffuse layers for A and X can continue to extend without constraint, this is not true. Therefore, the discrepancy of fluxes continues to grow as the region of maximum field "diffuses" to a region of lower diffusive flux, and the junction begins to discharge. All following behavior of the liquid junction is compensating for the charge separation generated before this point τ_{trs}, as a consequence of unequal diffusive fluxes on a nanosecond time scale.

The asymmetry of the junction with respect to X_{LJP} continues to develop as the discrepancy between migrational fluxes is always greatest at the junction center and less to either side, whereas the discrepancy in diffusional fluxes is maintained everywhere. The following concentration profiles (Figure 5) show that the continued relaxation of the field permits the approximate recovery of electroneutrality around the initial junction position; the reservoir of excess charge continues to diffuse down the concentration gradient. The electric field accelerates the following species to a sufficient extent that the $\tau \rightarrow \infty$ asymptote is attained and the junction discharges as $\tau^{1/2}$. Then, by the same capacitive argument as above

$$\frac{\partial \bar{Q}_{enc}}{\partial \Delta\theta_{LJP}} \frac{\bar{C}_d}{d} \quad \therefore \quad \Delta\theta_{LJP} \propto (\bar{Q}_{enc} \cdot d) \propto (\tau^{-1/2} \cdot \tau^{1/2}) \propto \text{constant} \tag{3.16}$$

The limiting constant potential difference across the liquid junction is therefore justified in terms of diffusion being the cause for both an increase in the mean distance of charge separation $\propto \tau^{1/2}$ and a decrease in the magnitude of that charge also $\propto \tau^{1/2}$, which in the limit $\tau \rightarrow \infty$ cancel precisely and cause a constant liquid junction potential. The system remains dynamic ($\partial c_i/\partial\tau \neq 0$), however; both species are continuously diffusing at a rate approaching the mean of their diffusion coefficients and the Nernst−Planck equations are not at steady state. The potential is only constant so long as diffusion continues unconstrained and so is only constant as long as the diffuse layer does not encounter some boundary where bulk solution is depleted. The system is also not locally electroneutral; it merely tends to electroneutrality in the infinite time limit. The potential difference is therefore associated with a finite charge separation which originates in the discrepancy in diffusive flux occurring at short times and under low electric field conditions, which is never fully compensated.

Of fundamental importance is that the constant limiting liquid junction potential for a free junction *only exists as a dynamic property* of the system, given that charge separation is entirely due to the initial conditions. It cannot be recovered from a static ($\partial c_i/\partial\tau = 0$) treatment, as in the classical solution, without the use of physically meaningless approximations or boundary conditions. This distinction is noted in the schematic at Figure 10.

3.3. Temporal and Spatial Extents of Type 1 Liquid Junctions. We have argued that type 1 liquid junctions approach a long time asymptote of constant potential difference across the junction, which is caused by the increased mean distance of charge separation in the junction exactly balancing the decrease in magnitude of separated charge. The time required to attain this limit is an unknown variable, however, and so was studied by simulation.

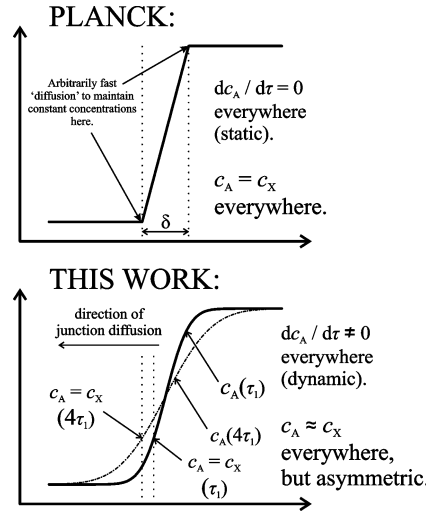

Figure 10. Schematic demonstrating the fundamentally different physical pictures entailed by Planck's static liquid junction and the dynamic model proposed in this work.

An appropriate time scale for the attainment of asymptotic behavior is that required for the system to achieve 99% of the potential difference predicted by the Henderson equation, defined as τ_{ss}:

$$\tau_{ss} = \tau(\Delta\phi_{LJP} = 0.99\Delta\phi_{Henderson}) \tag{3.17}$$

τ_{ss} additionally offers the most convenient parametrization for the spatial extent of a liquid junction: as ΔX_θ necessarily increases with the diffuse layer as long as increasing quantities of bulk solution are available, analysis of the spatial extent as an independent function of D'_A and c^*_L is only meaningful if a characteristic time is chosen at which it is considered. We therefore consider $\Delta X_{\theta,ss} = \Delta X_\theta(\tau = \tau_{ss})$.

The corresponding surface plots of τ_{ss} and $\Delta X_{\theta,ss}$, on a logarithmic scale, against D'_A and c^*_L, are shown in Supporting Information J.

In general, we note from these that a longer time scale is noted before asymptotic behavior is attained as c^*_L is increased; there is also a weak dependence on D'_A, such that where A and X have similar diffusion coefficients, a decreased equilibration time scale is noted. In both cases, then, a greater absolute liquid junction potential requires a longer time scale for that asymptotic constant potential to be achieved; the effect of concentration discontinuity is much greater than that of diffusion coefficient, however. The associated spatial extent changes correspondingly, as the diffuse layer associated with the liquid junction is in all cases larger at longer times.

Given that τ_{ss} is a function solely of D'_A and c^*_L, its dimensional analogue t_{ss} is additionally a function of k and D_X, according to eq 2.12. The time required for a liquid junction to attain its limiting potential is therefore inversely proportional to the product k^2D_X, and so is directly proportional to ε_s and inversely proportional to D_X and C^*_R. A solution of higher ionic strength or higher ionic mobility therefore achieves its limiting potential more rapidly as migration is accelerated. In a solution of higher permittivity, however, electric fields are screened to a greater extent. Consequently, the liquid junction is able to extend further before achieving a limiting potential difference, and so for a common ionic mobility its formation requires a longer time scale. These effects are demonstrated by plots of the dimensional values t_{ss} and x_{ss} at two ionic strengths for the model HCl system, again in Supporting Information J.

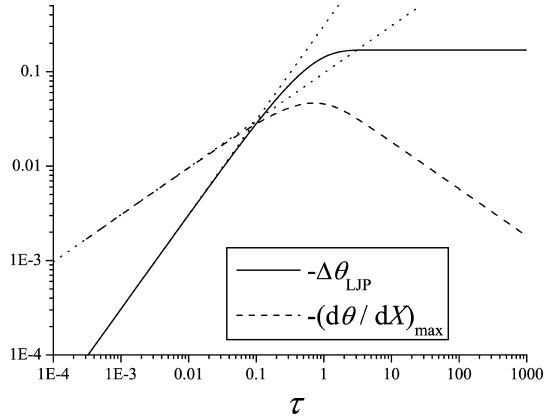

Figure 11. Dynamic evolution of liquid junction potential ($\Delta\theta_{LJP}$) and electric field ($-(\partial\theta/\partial X)_{max}$) for the type 2 junction of equimolar NaCl(aq) and KCl(aq), plotted on a logarithmic scale in time. Asymptotic limits derived using a zero-feedback approach plotted against the simulation data.

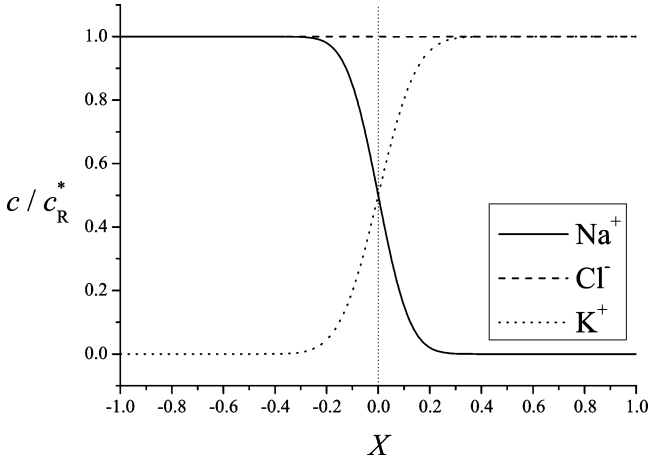

Figure 12. Concentration profile for the NaCl−KCl(aq) system at a time of $\tau = 0.01\tau_{trs}$ following junction formation. As at short time for type 1, the concentration profiles are symmetric and resemble the diffusion-only case; the diffuse layer associated with K^+ is more extensive than that of Na^+ due to differences in diffusion coefficient.

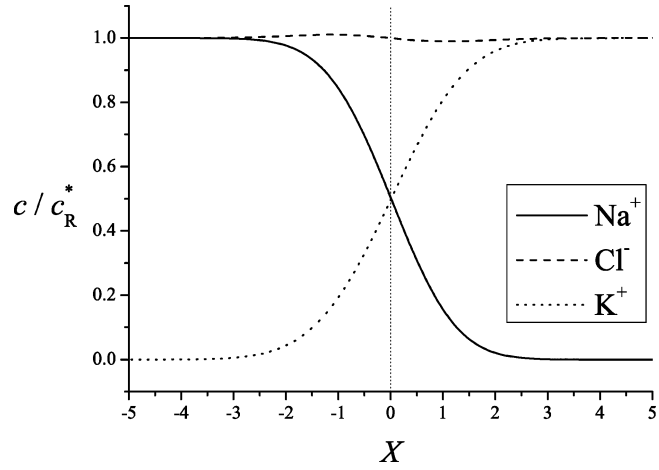

Figure 13. Concentration profile for the NaCl−KCl(aq) system at a time of $\tau = \tau_{trs}$ following junction formation. The concentration profile of X has become increasingly asymmetric under the influence of the electric field, and the point where $c_{Na^+} = c_{K^+}$ is now at $X < 0$.

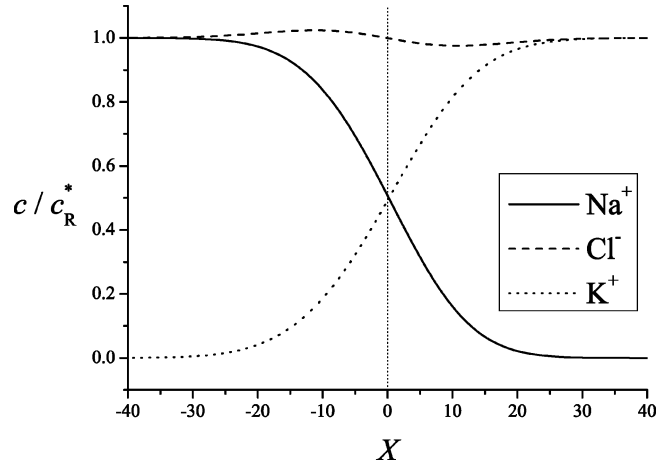

Figure 14. Concentration profile for the NaCl−KCl(aq) system at a time of $\tau = 100\tau_{trs}$ following junction formation. The asymmetry is further increased here and the point where $c_{Na^+} = c_{K^+}$ has shifted again to $X > 0$.

3.4. Dynamics of Liquid Junction Formation: An Exemplar Type 2 Junction with NaCl and KCl. The dynamical study of liquid junctions was extended to type 2 junctions by investigation of the junction between equally concentrated aqueous solutions of NaCl ($D'_{Na^+} = 0.6564$ at infinite dilution, 298 K) and KCl ($D'_{K^+} = 0.9631$ at infinite dilution, 298 K).[8]

3.4.1. Trends in $\Delta\theta_{LJP}$ and ξ_{max}. The essential trends in liquid junction potential and maximum electric field, as a function of time, are the same as for the type 1 case: a logarithmic plot is shown at Figure 11. We may therefore expect a similar physical rationalization of the steady potential across the liquid junction as in the type 1 case.

Some exemplar concentration profiles, across a similar logarithmic range on either side of τ_{trs} as in the type 1 case, are shown at Figures 12−14; $\tau_{trs} = 0.72 \approx 7$ ns in this case (for 10 mM solutions), at which time the maximum field is ≈0.3 MV m^{-1}. As in type 1, we observe approximately diffusional behavior at short time; longer times give greater asymmetry of the concentration profiles as the field extends. Interestingly, the point where $c_A = c_B$ deviates from $X = 0$ but not extensively. The corresponding evolution of the electric field profile, ξ, is shown in Figure 15; deviation of X_{LJP} away from $X = 0$ is not evident until $\tau > \tau_{trs}$ and then at lower magnitudes than in the type 1 example, where the variation in diffusion coefficients was much greater.

3.4.2. Asymptotic Analysis at $\tau \rightarrow 0$ by a Zero-Feedback Approximation. The $\tau \rightarrow 0$ limiting behaviors of the type 2 liquid junction may be approached by the zero-feedback approximation as for type 1. The mathematics are discussed in Supporting Information E, and the major results are

$$\left.\frac{\partial\theta}{\partial X}\right|_{max} \approx \frac{1}{\sqrt{\pi}}(\sqrt{D'_A} - \sqrt{D'_B})\cdot\sqrt{\tau} \qquad (3.18)$$

and

$$\Delta\theta_{LJP} \approx (D'_A - D'_B)\cdot\tau \qquad (3.19)$$

These are plotted as the $\tau \rightarrow 0$ asymptote in Figure 11, and again show excellent agreement with simulation in this limit.

3.4.3. Asymptotic Analysis as $\tau \rightarrow \infty$. Unfortunately, the simple long time asymptotic analysis in the type 1 case is not possible in the type 2 case. Hickman used a further perturbation involving the diffusion coefficients to achieve approximate results for this asymptote, and the mathematics here are discussed in their context in Supporting Information H.

The electric field is determined, to the first approximation, as

$$\frac{\partial\theta}{\partial X} \approx -\frac{2}{\sqrt{\pi\tau}}\frac{e^{-z^2}}{\gamma + \mathrm{erf}(z)} \tag{3.20}$$

where z is defined as above for type 1 and

$$\gamma = \frac{D'_B + D'_A + 2D'_X}{D'_B - D'_A} \tag{3.21}$$

This expression can be integrated to yield the type 2 Henderson equation; however, given the second perturbation required, the Henderson equation is not exact for type 2, even as $\tau \rightarrow \infty$.

A comparison of the electric field predicted by the Hickman theory with dynamic simulation is considered here for the first time. The comparison (plot in Supporting Information H) shows that the expression in eq 3.20 is a much less accurate description of the electric field in the system at $\tau = 100\tau_{trs}$ than was the case for the exact $\tau \rightarrow \infty$ treatment in the type 1 case. The position of the maximum field is poorly predicted, and the general asymmetric shape of the simulated field is not consistent with the Hickman theory, to the first approximation.

As above, we may differentiate the electric field to find the temporal evolution of X_{LJP}. As shown in Supporting Information H, this yields X_{LJP}, again being proportional to $s(\gamma)$, although here γ takes its type 2 definition as in eq 3.21. Comparison with simulation, however, shows that the analysis of X_{LJP} is very poor indeed; even the sign of the trend in X_{LJP} is incorrect, as simulation shows that the junction moves in the positive X direction at long times, whereas the opposite is predicted by our analysis. It is reasonable to assume in this case that although the accuracy of the Henderson equation (compared to simulation) implies that the integral of the higher terms in Hickman's approximation is negligible, these terms may be significant in the region of high field at the center of the junction, and so inherent asymmetries occurring in these higher terms will alter the dynamic trends in X_{LJP}.

3.4.4. Conclusion on Type 2 Dynamics. Simulation demonstrates that the dynamic trends in the maximum field and potential difference associated with a type 2 liquid junction are the same as those in type 1. Trends in ΔX_θ are also similar (Supporting Information I).

A small time limit where the electric field may be neglected exists, and a straightforward zero-feedback analysis gives results identical to the $\tau \rightarrow 0$ trends observed in the simulation of a model (NaCl−KCl) system. The unequal rates of diffusion of Na^+ and K^+ in opposing directions causes a charge separation and hence a potential difference that develops as τ. As the electric field develops, it retards the diffusion of the faster species and accelerates the diffusion of the slower species. The electric field at the junction position achieves a maximum in time when the fluxes of all species are zero, and this again occurs on the 5−50 ns time scale for typical concentrations of electrolyte.

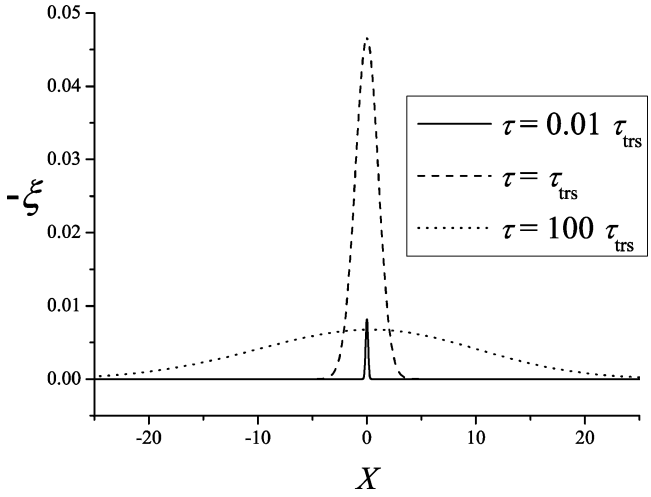

Figure 15. Evolution of the electric field profile for the NaCl−KCl(aq) system at times $\tau = 0.01\tau_{trs}$ to $\tau = 100\tau_{trs}$ following junction formation. Increased asymmetry of the initial junction position is evident; close analysis shows that the liquid junction position, X_{LJP}, is varying.

As in type 1, the nonuniformity of the electric field causes asymmetry in the concentration profiles due to varying rates of retardation or acceleration of the diffusion. In particular, the concentration profile of the common ion species X ceases to be uniform. These asymmetries cause overall movement of the position of the liquid junction, which in the type 2 case is not well accounted for by asymptotic theory. Empirical evidence from simulation shows a long time $\tau^{1/2}$ diffusion of the junction position, but with a coefficient that differs by a factor of −1/2 from that predicted by the approximate theory, which although it correctly predicts the Henderson equation in its leading term is clearly inadequate as a general description of the electric field in this case.

Again, it is evident that the steady liquid junction potential can be rationalized on the basis of the expansion of the junction in time occurring at a rate proportional to $\tau^{1/2}$, which balances the loss of charge in the junction also proportional to $\tau^{1/2}$, such that a constant potential difference arises as an exclusively dynamic property of the system.

3.5. Temporal and Spatial Extents of Type 2 Liquid Junction Potentials. Plots for τ_{ss} and $\Delta X_{\theta,ss}$ were produced for type 2 junctions, using the same definitions as in section 3.3, and are shown in Supporting Information J.

In general, greater absolute diffusion coefficients accelerate all mass transport processes and hence accelerate the rate of attainment of asymptotic behavior. This is also apparently accelerated where the limiting liquid junction potential itself is relatively small, i.e., where D_A and D_B are similar. The same arguments concerning the effects of the dimensional parameters contained within the scaling factor k apply as in the type 1 case, above (section 3.3).

Junction extent increases with magnitude of the potential difference and also with relative values for diffusion coefficient, as expected for the larger diffusion layers associated with more mobile species, causing charge separation over a wider extent.

We note that as the Henderson equation, which is approximate, was used to define τ_{ss} and $\Delta X_{\theta,ss}$ here. The error in the Henderson equation is greater where $\Delta\theta_{LJP}$ is larger, and so the dependence on the magnitude of the potential difference in these plots is possibly an artifact. We intend to investigate this more fully by finding a more appropriate definition for τ_{ss} in the type 2 case.

4. Conclusions

We have analyzed liquid junctions of Lingane's types 1 and 2 (Figure 1) using Nernst−Planck−Poisson numerical simulation, with boundary conditions that avoid the physical inconsistencies with the laws of conservation of mass and charge identified in the traditional literature.[14] The numerical simulation approach allows the construction of a general physical picture of the dynamic evolution and short- and long-time behaviors of the liquid junctions. In particular, we present a validation of the asymptotic analysis performed by Hickman[15] and Jackson[16] in the early 1970s; work which has not been considered in computational studies of the liquid junction dating from the

modern era[18−20,14] when accurate simulation of the NPP equations, an extremely computationally demanding procedure, has become viable.

Our concept of the liquid junction is a synthesis of novel computational and mathematical study and the aforementioned asymptotic analysis. The steady *liquid junction potential* results from charge separation engendered by unequal rates of diffusion. This charge separation causes an electric field that modulates the unequal transport of species, within a few nanoseconds for the majority of systems, and allows the liquid junction to begin to discharge toward its *equilibrium* state of electroneutrality throughout the system. This state is not achieved until infinite time, however; continuing diffusion causes the junction to grow at a rate equal and opposite to its rate of discharge, such that a steady potential difference arises. The steady potential arises at time scales of 10−1000 ns after junction formation for typical aqueous systems, by which time the diffuse layer is approximately 10−1000 nm in extent, and is continuously expanding at a rate proportional to $\sqrt{\tau}$.

The only steady state of the system, i.e., a state where the time derivatives of all species concentrations everywhere in space is zero, is the equilibrium where concentrations are constant across all space. So long as the diffuse layer encounters no finite boundaries, this equilibrium is not attained at any time less than infinity from initial conditions of step functions in concentration. The diffusion of the slower species never entirely catches up with the faster species, although as time tends to infinity the system becomes increasingly indistinguishable from its equilibrium state; the charge separation is, however, forever nonzero and so a finite potential difference across the junction is physically acceptable.

Therefore, our principal new physical insight is that constant free liquid junction potentials arise as *dynamic* properties of the system. Any attempt, as common in the traditional literature,[4] to derive the unconstrained liquid junction potential on the basis of a *static* system, where the Nernst−Planck equations may be taken at such a steady state and hence integrated, must necessarily contain some inconsistency with known laws of physics such as conservation of mass or charge. The static model, unlike the dynamic model, hence does not represent a valid physical picture of the liquid junction potential.

Acknowledgment. E.J.F.D. thanks St John's College, Oxford, for funding. L.F. thanks the Studienstiftung des deutschen Volkes for funding and Pembroke College, Oxford, for enabling his work in the Physical and Theoretical Chemistry Laboratory. E.J.F.D. additionally thanks Yvann Young and Helena Dickinson for their assistance with the German−English translation.

Supporting Information Available: (A) A summary of the arguments made by Planck in his original work treating liquid junctions with a static boundary layer approximation; (B) details of the numerical methods employed to solve the Nernst−Planck−Poisson equations dynamically, and of the mathematics of the iterative Newton−Raphson method used to numerically solve the nonlinear equations in this paper; (C) plots showing simulated liquid junction potentials once a steady limiting value has been attained, and their comparison with the Henderson equation; (D) asymptotic analysis of the type 1 system as $\tau \rightarrow 0$, including empirical analysis of the dynamic variation of X_{LJP} in this limit; (E) asymptotic analysis of the type 2 system as $\tau \rightarrow 0$; (F) mathematical details of the Boltzmann transformation of the Nernst−Planck−Poisson equations; (G) summarized and clarified mathematical details of the asymptotic analysis of Hickman and Jackson as $\tau \rightarrow \infty$ for type 1, including our own comparisons with simulation and novel analysis of the dynamic variation of X_{LJP} in this limit; (H) summarized and clarified mathematical details of the asymptotic analysis of Hickman as $\tau \rightarrow \infty$ for type 2, including our own comparisons with simulation and novel analysis of the dynamic variation of X_{LJP} in this limit; (I) dynamic trends in ΔX_θ for type 2; (J) plots showing the temporal and spatial extents of type 1 and type 2 liquid junctions. This material is available free of charge via the Internet at http://pubs.acs.org.

References and Notes

(1) Lingane, J. J. *Electroanalytical Chemistry*, 2nd ed.; Wiley: New York, 1958.
(2) Nernst, W. H. *Z. Phys. Chem.* **1889**, *4*, 165.
(3) Planck, M. *Wied. Ann.* **1890**, *39*, 161–186.
(4) Planck, M. *Wied. Ann.* **1890**, *40*, 561–576.
(5) In the case of a finitely positioned impermeable membrane, however, the liquid junction potential is not constant and an attainable equilibrium of zero concentration gradient exists, where the liquid junction potential is zero (cf. ref 14). However, if the membrane is permeable to any species, the diffuse layer outside that membrane must be considered. Finitely positioned Dirichlet conditions are therefore to our minds unphysical for any system, excepting the imposition of a convectional Nernst layer.
(6) Henderson, P. *Z. Phys. Chem.* **1907**, *59*, 118–127.
(7) Henderson, P. *Z. Phys. Chem.* **1908**, *63*, 325–345.
(8) Bard, A. J.; Faulkner, L. R. *Electrochemical Methods: Fundamentals and Applications*, 2nd ed.; John Wiley & Sons: New York, 2001.
(9) Guggenheim, E. A. *J. Am. Chem. Soc.* **1930**, *52*, 1315–1337.
(10) Hafemann, D. R. *J. Phys. Chem.* **1965**, *69*, 4226–4231.
(11) Bagg, J. *Electrochim. Acta* **1990**, *35*, 361–365.
(12) Bagg, J. *Electrochim. Acta* **1990**, *35*, 367–370.
(13) Bagg, J. *Electrochim. Acta* **1992**, *37*, 719–723.
(14) Perram, J. W.; Stiles, P. J. *Phys. Chem. Chem. Phys.* **2006**, *8*, 4200–4213.
(15) Hickman, H. J. *Chem. Eng. Sci.* **1970**, *25*, 381–398.
(16) Jackson, J. L. *J. Phys. Chem.* **1974**, *78*, 2060–2064.
(17) Buck, R. P. *J. Membr. Sci.* **1984**, *17*, 1–62.
(18) Skryl, Y. *Phys. Chem. Chem. Phys.* **2000**, *2*, 2969–2976.
(19) Sokalski, T.; Lewenstam, A. *Electrochem. Commun.* **2001**, *3*, 107–112.
(20) Sokalski, T.; Lingenfelter, P.; Lewenstam, A. *J. Phys. Chem. B* **2003**, *107*, 2443–2452.
(21) Goldman, D. E. *J. Gen. Physiol.* **1942**, *27*, 37.
(22) Goldberg, R. N.; Frank, H. S. *J. Phys. Chem.* **1972**, *76*, 1758–1762.
(23) Morf, W. E. *Anal. Chem.* **1977**, *49*, 810–813.
(24) Brumleve, T. R.; Buck, R. P. *J. Electroanal. Chem.* **1978**, *90*, 1–31.
(25) Brumleve, T. R.; Buck, R. P. *J. Electroanal. Chem.* **1981**, *126*, 55–71.
(26) Mafé, S.; Pellicer, J.; Aguilella, V. M. *J. Phys. Chem.* **1986**, *90*, 6045–6050.
(27) Horno, J.; Castilla, J.; Gonzalez-Fernandez, C. F. *J. Phys. Chem.* **1992**, *96*, 854–858.
(28) Martuzans, B.; Skryl, Y. *J. Chem. Soc., Faraday Trans.* **1998**, *94*, 2411–2416.
(29) Josserand, J.; Lagger, G.; Jensen, H.; Ferrigno, R.; Girault, H. H. *J. Electroanal. Chem.* **2003**, *546*, 1–13.
(30) Park, J.; Huh, K. Y.; Li, X. *J. Electroanal. Chem.* **2006**, *591*, 141–148.
(31) Filipek, R.; Szyskiewicz-Warzecha, K.; Bozek, B.; Danielewski, M.; Lewenstam, A. *Defect Diffus. Forum* **2009**, *283−286*, 487–493.

JP908024S